Design and analysis of a 2D photonic crystal based parallelogram-shaped cavity with open corners for optical switching

NRG Sreevani[1], *T Annalakshmi*[2*], and *V R Balaji*[3]

[1]Department of Computer Science and Engineering, S.A. Engineering College, Chennai, Tamil Nadu, India
[2]Department of Electronics Communication and Engineering, S.A. Engineering College, Chennai, Tamil Nadu, India
[3] School of Electronics Engineering, Centre for Healthcare Advancement, Innovation and Research, Vellore Institute of Technology, Chennai, Tamil Nadu, India

Abstract. In this paper, we designed a 2×2 optical switch using a two-dimensional photonic crystal (2D PC) based on interference principle. For the first time, an air-hole slab-structure-based photonic switch is proposed. The proposed optical switch consists of input and output bus waveguides connected by an open-corner parallelogram-shaped cavity that effectively controls light flow using interference. The propagation of electromagnetic waves is analysed using the finite-difference time-domain (FDTD) method. The proposed photonic crystal switch exhibits an ultrafast response time of 1.27 ps, supporting a data rate of up to 0.78 Tbps, with maximum crosstalk of −5.79 dB for cross state and -27 dB for bar state. Hence, the proposed photonic switch is suitable for high-speed switching applications.

1 Introduction

Photonics is an emerging technology that offers high speed, low loss, and high bandwidth to overcome the limitations of traditional electronic systems [1]. Photonic-based devices use light to carry the information and manipulate it for applications in communication [2], sensing [3], and signal processing [4]. Photonic materials are periodic nanostructures with a modulated refractive index which allow precise control and manipulation of the light propagation at the nanoscale. These materials are classified into one dimension (1D), two dimensions (2D), and three dimensions (3D) based on the periodic variation of refractive index. Such materials prevent the propagation of light within a specific wavelength range within the structure, called the Photonic Bandgap (PBG) [5]. However, introducing defects in the PC allows the control light to propagate within the PBG region. Due to the aforementioned parameters, many optical devices such as logic gates [6], demultiplexer [7], circulators [8], routers [9], and switches [10-12].

* Corresponding author: drannalakshmi@saec.ac.in

Photonic switches are used to control and redirect optical signals in optical communication networks and Photonic Integrated circuits. Researchers have already reported photonic switches in microring resonators [13], Mach-Zehnder interferometers [14], and direction couplers [15]. However, these technologies suffer from large device size, higher power consumption, bandwidth limitation, high crosstalk, and limited data rate. In contrast, 2D PC-based photonic switches can efficiently control and route light, provide high data rates, low loss, and low crosstalk, and offer a very compact size [16].

In earlier studies, 2D PC-based switches have been reported using Square-shaped ring resonators [10] and octagonal-shaped ring resonators [11] are designed using rod-type structures. All these works are closed cavities that contain sudden transitions at sharp corners and have too high scattering losses. In this work, we propose an optical switch based on an open-corner parallelogram-shaped cavity using an air-hole slab structure. This proposed shape reduces the loss of sharp corners and provides a smooth transition between bar and cross states. The air hole radius of the entire structure is uncertain, which simplifies the design complexity and tolerance. Importantly, to our knowledge, no optical switch in 2D PC is reported using an air hole slab structure, which can be fabricated easily with current technology [17].

The rest of the paper is discussed as follows. Section 2 presents the photonic bandgap analysis of the proposed structure. Section 3 describes the design structure and working principles of the cross-and-bar state switch. The results and discussion of the proposed structure are explained in Section 4. Finally, the conclusion of the work is given in the final section.

2 Photonic bandgap analysis

A Photonic switch is designed using an air-hole slab structure with 25 air holes along the X direction and 21 air holes along the Z direction. The background material is silicon, with a refractive index of 3.476 at a centre wavelength of 1550 nm, and the component material is air arranged in a hexagonal lattice. Fig. 1 shows the hexagonal lattice before introducing defects, and the contour profile of the proposed lattice is shown in Fig. 2. The red colour represents the silicon background, and the violet colour represents the air holes.

The periodic modulation of RI in the PC allows only specific wavelengths to propagate through the structure while reflecting other wavelengths, resulting in the formation of a photonic bandgap (PBG). The PBG is determined using the plan wave expansion (PWE) method, which solves Maxwell's equations to determine the forbidden frequency regions of the periodic structure [18].

$$\nabla \times \left(\frac{1}{\varepsilon_r(x,y)} \nabla \times \mathrm{E}(x,y) \right) = \left(\frac{\omega}{c} \right)^2 E(x,y) \tag{1}$$

High refractive index contrast in the air hole slab geometry restricts the optical propagation to transverse electric (TE) polarized modes, while other polarization modes are scattered out of the slab. The proposed photonic switch is designed on a silicon-on-insulator (SOI) platform. The device consists of a 220 nm-thick silicon device layer, a silicon dioxide layer that reduces optical leakage and noise, and a 500 μm-thick silicon handling layer. To observe the PBG within the optical communication window, the lattice constant is chosen as 410 nm and air hole radius is optimized to 135 nm, which covers the communication (C) band optical window. With these optimized structural parameters, plane wave expansion (PWE) method determines the first TE bandgap in the normalized frequency range of 0.217

<a/λ< 0.317, which corresponds to wavelengths from 1293 nm to 1889 nm. The second bandgap appears in the range 0.61 < a/λ < 0.65 and at wavelengths from 630 nm to 672 nm, which are outside the optical wavelength region. The proposed photonic switch is designed to operate in the optical region, and the first TE bandgap is used for further analysis.

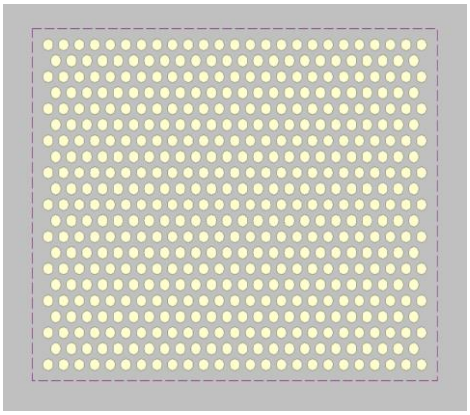

Fig. 1. Hexagonal PC lattice with 25×21 air hole array

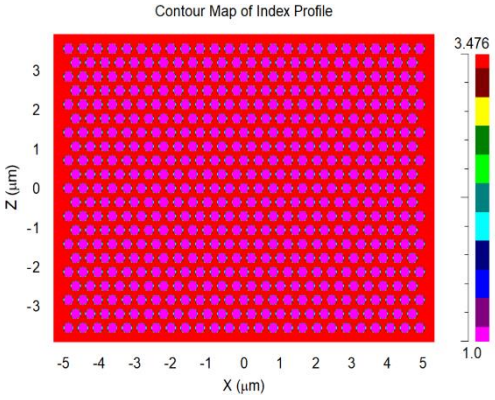

Fig. 2. Contour profile of the proposed PC structure.

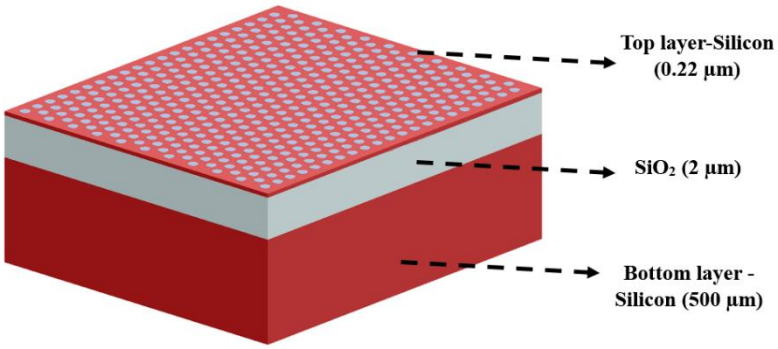

Fig. 3. Schematic view of the SOI slab

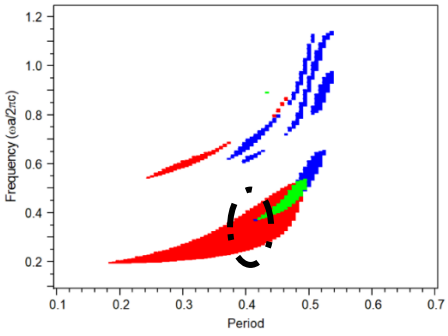

Fig. 4. Bandgap analysis of Period and Normalized frequency

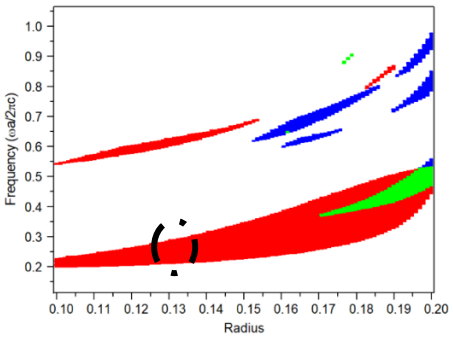

Fig. 5. Bandgap analysis of Radius and Normalized frequency

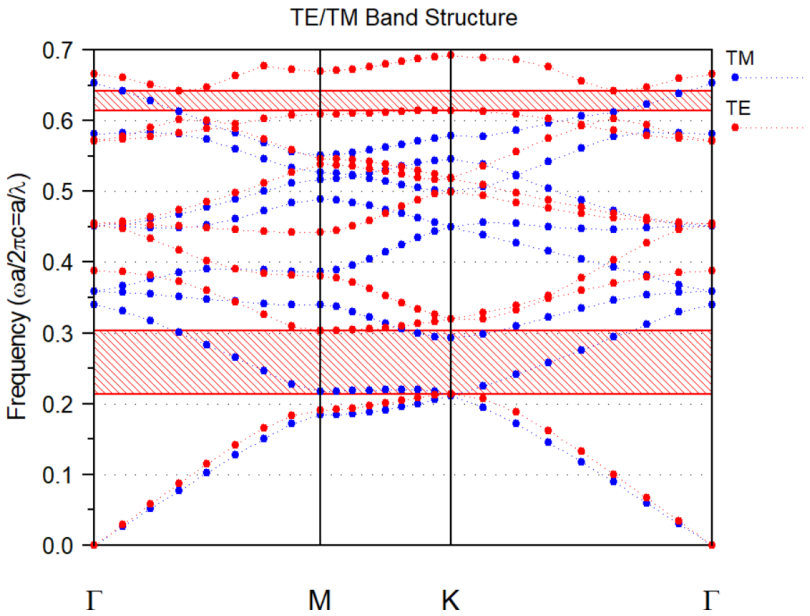

Fig. 6. Band diagram for the proposed lattice before introducing the defects

2.1 Structural design of the parallelogram-shaped defect switch

The proposed switch is designed to operate in cross and bar states is shown in Fig.7. At the resonance wavelength, it switches functions as a cross-state. It couples light efficiently between the waveguides and redirects it by 90 °. In the bar state light propagate along the straight waveguide. [19]

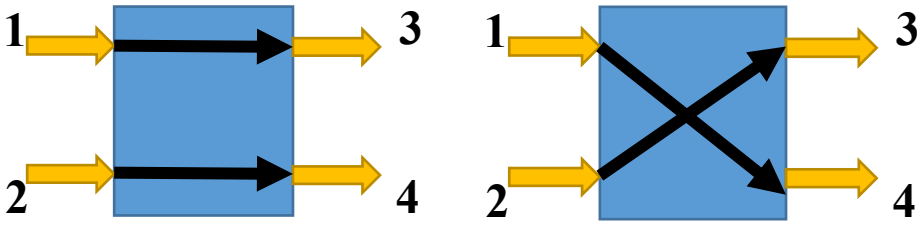

Fig. 7. Logic of Bar state and Cross state switch

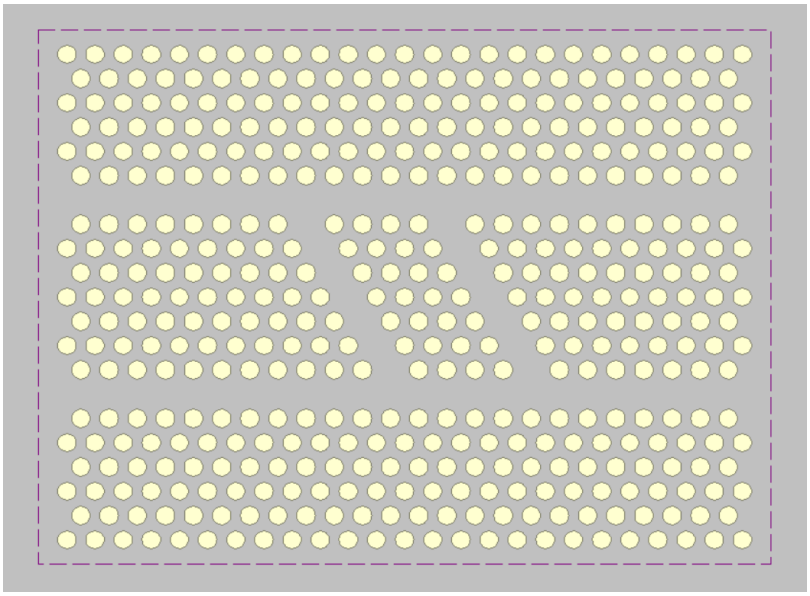

Fig. 8. Schematic view of the proposed modified parallelogram-based 2D PC switch

Figure 8 shows the schematic view of the proposed switch using a parallelogram-shaped open-defect cavity (SODC). The two straight-line defect waveguides are formed by removing air holes from the PC lattice. These waveguides are designed to have two input and output ports, allowing light to enter and exit in different directions according to the interference principle. The central region is a parallelogram SODC, created by removing the air holes and the cavity corners to connect the input and output ports. The waveguides cross at a tilted, parallelogram shaped open area called a defect region. These regions allow the light from either input port to enter the defect area and split into different propagation paths. The light bends within the region due to interference, and it can travel straight or bend towards the output port. The footprint of the photonic switch is 60 μm2, which is compact and practical for on-chip photonics switching applications.

3 Simulation results and discussion

The two-dimensional finite-difference time-domain (2D FDTD) algorithm is used to analyse the propagation of electromagnetic waves within the structure. A TE-polarized continuous-wave (CW) light source with a wavelength of 1550 nm is launched into the input waveguide. The power monitors are placed at the end of each waveguide to monitor the normalised transmitted power in both the time and wavelength domains. Perfectly matched layer (PML) boundaries are used around the simulation region to absorb outgoing waves and reduce unwanted reflections [19].

$$P(t) = \frac{\mathrm{Re}\left[\int_A \left[E(t) \times H^*(t)\right] dA\right]}{\mathrm{Re}\left[\int_A \left[E(t_0) \times H^*(t_0)\right] dA\right]} \tag{2}$$

FDTD simulation uses a grid size of 0.01 μm in all directions, with 10 points per effective wavelength to ensure accurate results. The simulation region extends from −11.582 μm to +11.582 μm in the x-direction and from −4.7934 μm to +4.7934 μm in the z-direction. A two-dimensional y-cut model is considered for the analysis. The time step is selected as 0.016 fs to satisfy the Courant–Friedrichs–Lewy stability condition [20], and the simulation is run for 10000 time steps.

$$\Delta t \leq \frac{1}{c\sqrt{\frac{1}{\Delta x^2} + \frac{1}{\Delta y^2}}} \tag{3}$$

In case 1, the light is launched only at input port 1, and no light is launched at input Port 2. For this input configuration, the obtained output powers in the cross-state logic are 0.91 at Port 4 and 0.2 at Port 4. During the on-resonance wavelength (1550.6 nm), constructive interference occurs along the coupling path towards Port 4, while destructive interference suppresses the transmission toward Port 3. Significant optical light signal is redirected to Port 4, and a small fraction of power is coupled to Port 3 as shown in Fig. 9 and Fig. 10. The current logic exhibits a response time of 1.73 ps, a data rate of 0.58 Tbps, and a crosstalk level of -5.79 dB as shown in Table.1 and Table.2. In Case 2, with the same input logic as Case 1, the device operates at a wavelength of 1538.6 nm, where light bypasses the cross cavity and reaches Port 3 as shown in Fig.11and Fig.12. Hence, the switch operates in the bar state. The proposed logic exhibits a response time of 0.133 ps, a data rate of 7.52 Tb/s, and a crosstalk level of −27 dB. The light was launched in the port 1, due to on resonance light is redirected to Port 4 and less power coupled to Port 3, as shown in Fig.9&Fig.10.The response time of 1.73 ps and data rate of 0.58 and cross talk of -5.79 dB

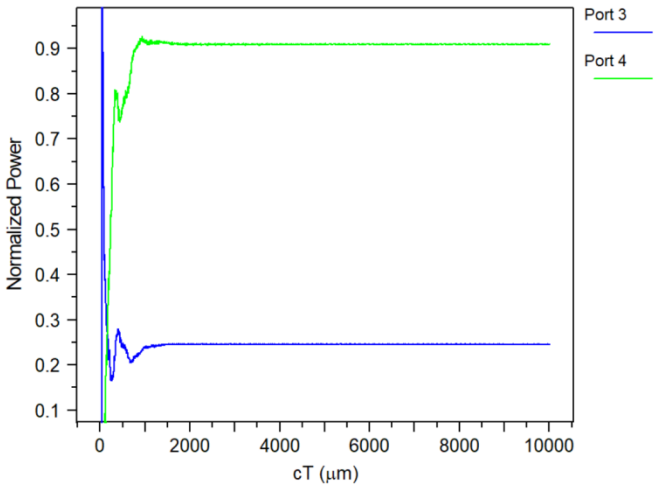

Fig. 9. Time spectra for the cross state with input 10 and output 01 (λ=1550.6 nm)

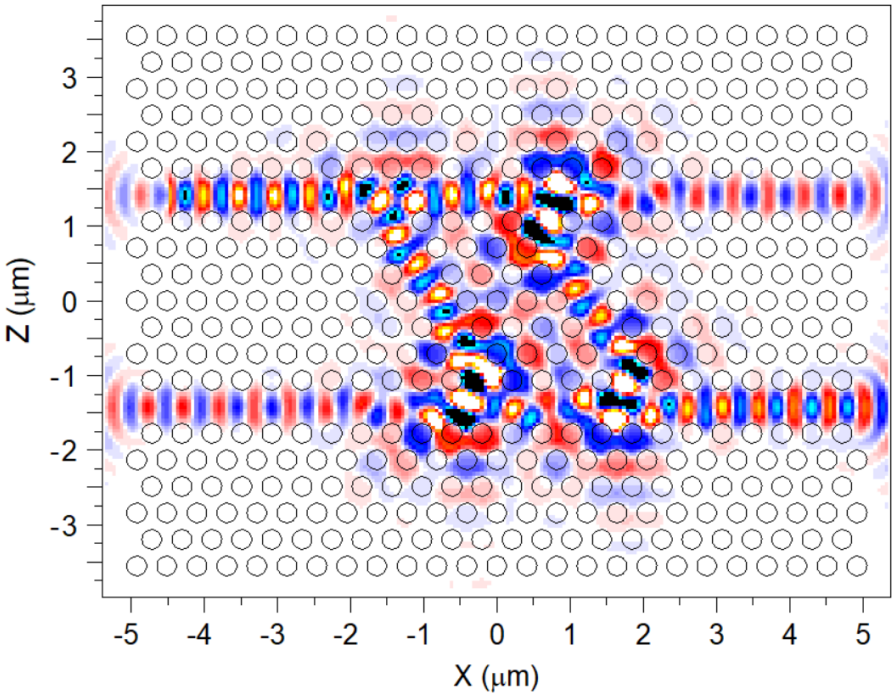

Fig. 10. Electric field distribution for the cross state with input 10 and output 01

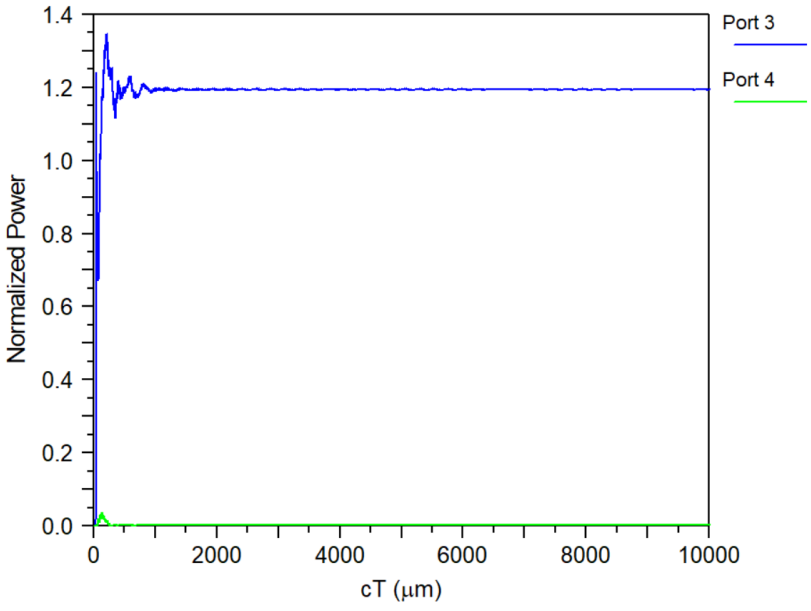

Fig. 11. Time spectra for the Bar state with input 10 and output 10 (λ=1538.6 nm)

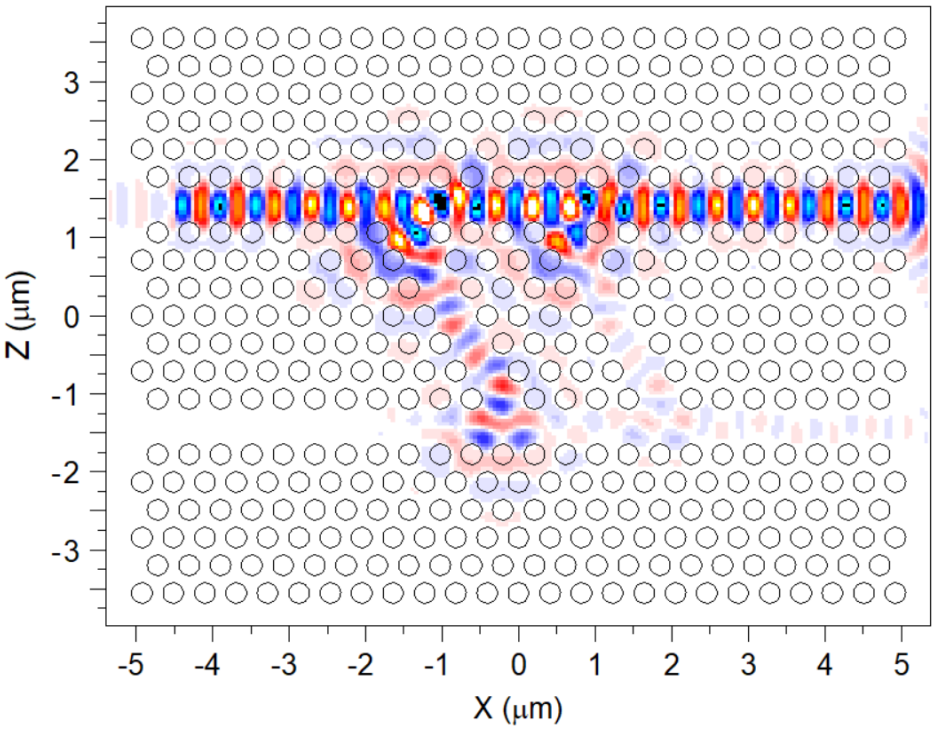

Fig. 12. Electric field distribution for the Bar state with input 10 and output 10

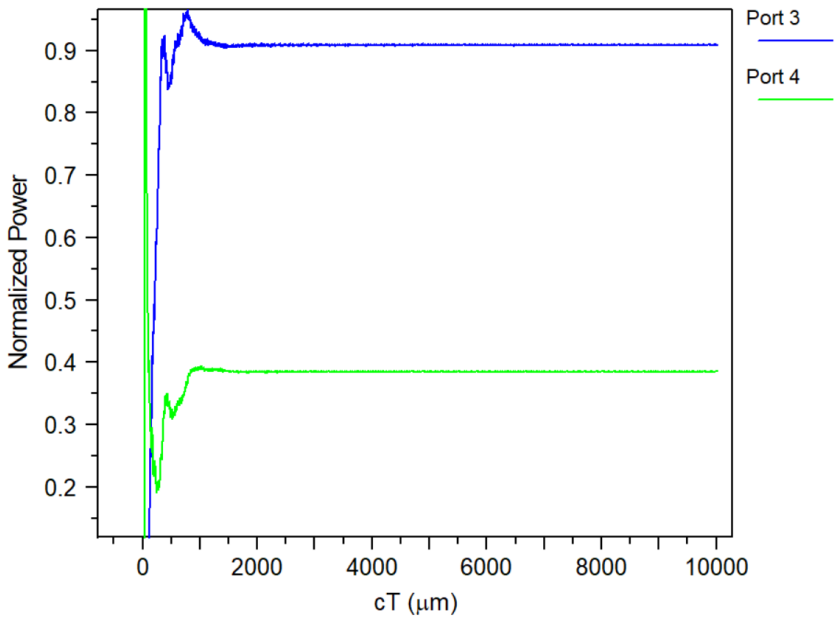

Fig. 13. Time spectra for the cross state with input 01 and output 10 (λ=1551.2 nm)

In case 3, the light is launched only at input port 2. At the on-resonance wavelength of 1551.2 nm, constructive interference directs the majority of the optical signal toward Port 3, while destructive interference reduces the transmission to Port 4. The output powers are 0.90 at Port 3 and 0.38 at Port 4, which determine effective signal routing according to the cross-state logic. This behaviour confirms that the device can selectively control light propagation between output ports for a given input logic. The switch exhibits a fast response time of 1.27 ps, a data rate of 0.78 Tb/s, and a crosstalk of -3.74 dB, indicating reliable isolation between ports and suitability for high-speed optical switching applications, compared to reported works.

In Case 4, for the same input logic as Case 3, the device operates at a wavelength of 1582.4 nm, corresponding to the off-resonance condition. As a result, the light does not enter the cross cavity and propagates straight to Port 4 as shown in Fig.15 and Fig.16. Hence, the switch operates in the bar state. The proposed logic exhibits a response time of 0.1 ps, a data rate of 10 Tb/s, and a crosstalk level of −22 dB. These results highlight the potential of the proposed switch for ultrafast optical networks, where precise control and minimal interference are essential.

The proposed parallelogram-shaped cavity with open corners improves performance by mitigating the effects of sharp corners observed in reported square and octagonal cavity designs. In earlier works, closed cavities contain sudden 90^0transiitons at the corners. These sharp corners cause strong light scattering, radiation loss and reflections. In the proposed design, the open corner parallelogram shape reduces these sudden transitions. This cavity is not fully closed and lacks sharp corners, so light can propagate more smoothly within the structure. This reduces scattering losses and improves light propagation between the bar and cross states.

Table 1. Performance parameters for 2×2 optical switch

State	**Input ports**		**Propagation Time (cT)(um)**			**Response time (ps) (T)**
	1	**2**	**10%**	**90%**	**90%-10%**	
Cross state	1	0	100	620	520	1.73
	0	1	120	500	380	1.27
Bar state	1	0	40	80	40	0.133
	0	1	30	60	30	0.10

Table 2. Data rate, Crosstalk for proposed 2 × 2 switch

State	**Input ports**		**Output ports**		**Response time (ps)**	**Data rate (Tbps)**	**Crosstalk (dB)**
	1	**2**	**3**	**4**			
Cross state	1	0	0.24	0.91	1.73	0.58	-5.79
	0	1	0.90	0.38	.1.27	0.78	-3.74
Bar state	1	0	1.192	0.002	0.133	7.52	-27
	0	1	0.006	1.04	0.10	10	-22

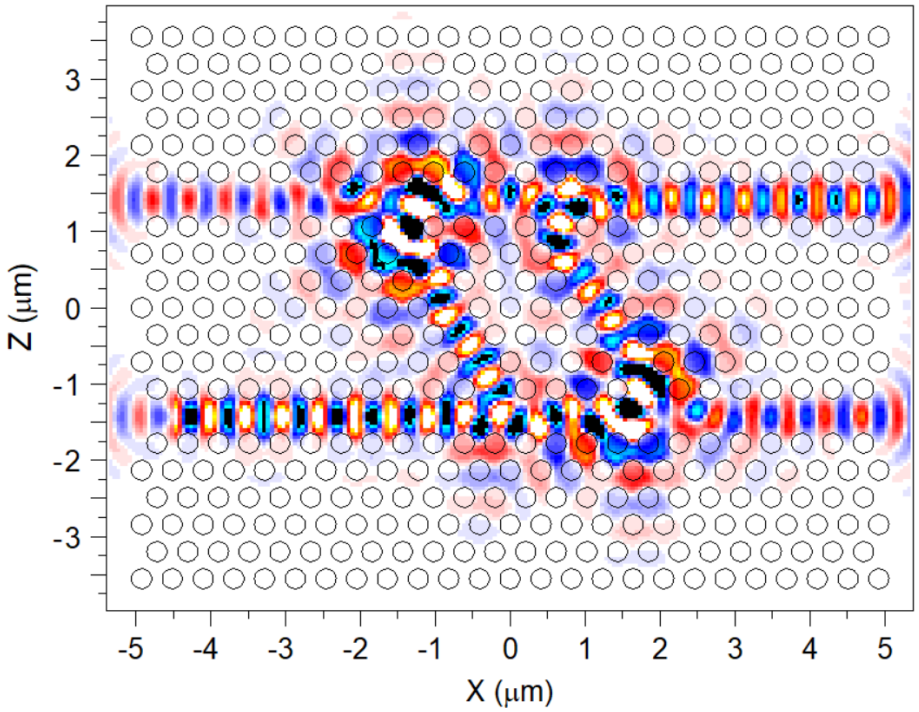

Fig. 14. Electric field distribution for the cross state with input 01 and output 10

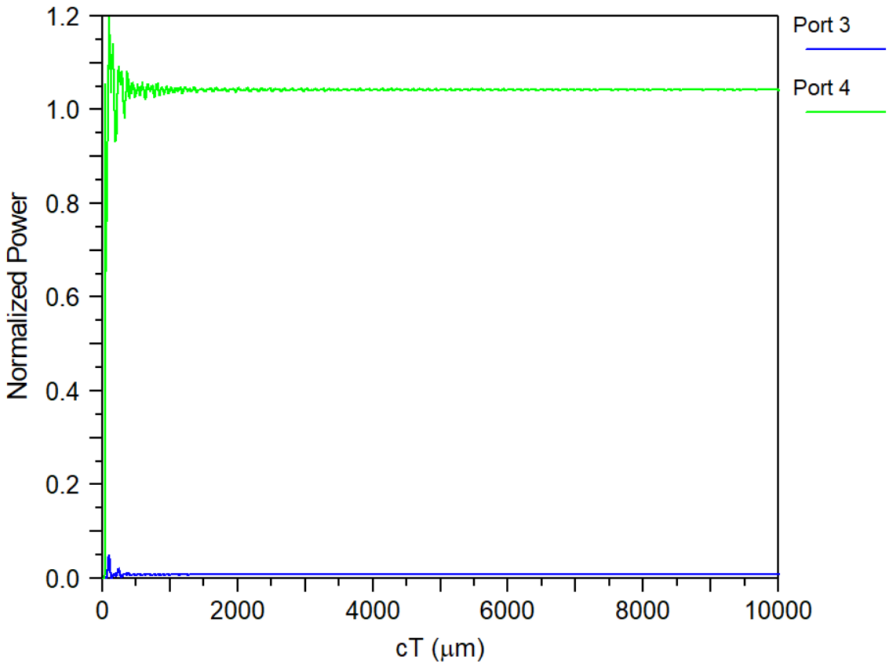

Fig. 15. Time spectra for the Bar state with input 01 and output 01 (λ=1582.4 nm)

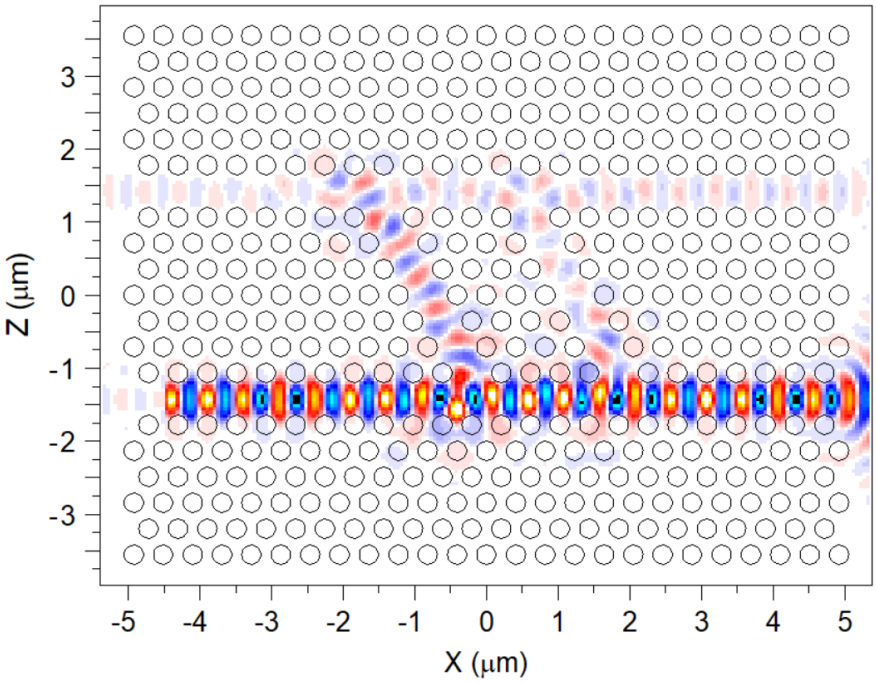

Fig. 16. Electric field distribution for the Bar state with input 01 and output 01 (λ=1582.4 nm)

The proposed device can be fabricated using Electron Beam Lithography (EBL) , which provides the high resolution required for nanoscale patterning. The structural parameters for the design are a lattice constant of 410 nm and a minimum air-hole diameter of 260 nm, within the resolution capability of EBL.

Due to the sub-100 nm feature requirements, techniques such as nanoimprint lithography, interference lithography, and conventional photolithography may not provide sufficient precision or alignment accuracy for this design. Therefore, EBL is the most suitable fabrication method [21]. The proposed structure is relatively simple, consisting of two line defects (one at the top and one at the bottom) and two 60° diagonal defects in the central region. This geometry maintains lattice symmetry and facilitates controlled light propagation within the photonic crystal slab.

The design has been tested for fabrication tolerances, and it operates successfully with dimensional variations of ±3 nm without altering the operating principle. This demonstrates good robustness against minor fabrication deviations.

4 Conclusion

In this work, a 2×2 photonic switch is designed on an air hole slab structure. To the best of our knowledge, no prior studies have reported a photonic switch using an air-hole slab. The structure uses a single air-hole radius, which simplifies the design and fabrication process. The switch achieves a high data rate of 1 Tbps with low crosstalk of -27 dB. The cross-state performance parameters of the proposed switch required further improvement and will be addressed in future work. The proposed switch is suitable for high-speed, low-power, and on-chip optical computing applications.

References

1. A. Nicolas, J.-L. Barrat, J. Rottler, Effects of inertia on the steady-shear rheology of disordered solids. Phys. Rev. Lett. **116**, 058303 (2016).
2. C. Xiang, S. M. Bowers, A. Bjorlin, R. Blum & J. E. Bowers, Perspective on the future of silicon photonics and electronics. Appl. Phys. Lett. 118, 22 (2021).
3. A. Boes, L. Chang, C. Langrock, M. Yu, M. Zhang, Q. Lin, & A. Mitchell, Lithium niobate photonics: Unlocking the electromagnetic spectrum. Sci., 379, 6627 (2023) eabj4396.
4. V. M. Passaro, C. De Tullio, B. Troia, M. La Notte, G. Giannoccaro, & F. De Leonardis, Recent advances in integrated photonic sensors. Sens, 12(11), 15558-15598 (2012).
5. J. Capmany, J. Mora, I. Gasulla, J. Sancho, J. Lloret, & S. Sales, Microwave photonic signal processing. J. Lightwave Technol, 31(4), 571-586 (2012).
6. E. J. J. B. Yablonovitch, Photonic band-gap structures. JOSA B, 10(2), 283-295 (1993).
7. A. Salmanpour, S. Mohammadnejad, & A. Bahrami, Photonic crystal logic gates: an overview. Opt. Quantum Electron**.** 47(7), 2249-2275 (2015).
8. V. R. Balaji, M. Medha, E. H. Shaik, A. Sivasubramanian, N. Ali, G. Hegde, & G. Vinitha, Design and Analysis of a Photonic Crystal DWDM Demultiplexer using an Overlap Ring Cavity to Drop Narrow Linewidth Channels. Silicon, 1-22 (2025).
9. D. S. Sundar, C. Umamaheswari, T. Sridarshini, M. Karthikeyan, R. Sitharthan, A. S. Raja, & M. F. Carrasco, Compact four-port circulator based on 2D photonic crystals with a 90 rotation of the light wave for photonic integrated circuits applications. Laser Phys. 29(6), 066201 (2019).
10. J. Yuan, J. Yang, D. Shi, W. Ai, & T. Shuai, Design optimization of a low-loss and wide-band sharp 120 waveguide bend in 2D photonic crystals. Opt. Commun.367, 356-363 (2016).
11. B. S. Thankaraj, A. Ramasamy, & B. V. Rajarajan, Beam steering permutation switch using annular photonic crystal for optical networks. J. Opt., 27(5), 055002 (2025).
12. R. Rajasekar, G. T. Raja, & S. Robinson, Numerical investigation of reconfigurable photonic crystal switch based on phase change nanomaterial. IEEE Transactions on Nanotechnology. 19, 545-552 (2020).
13. M. K. Chhipa, B. T. P. Madhav, & B. Suthar, An all-optical ultracompact microring-resonator-based optical switch. J. Comput. Electron**.** 20(1), 419-425 (2021).
14. S. Kumar, S. K. Raghuwanshi, & A. Kumar, Implementation of optical switches using Mach–Zehnder interferometer. Opt. Eng. 52(9), 097106-097106 (2013).
15. S. Han, T. J. Seok, N. Quack, B. W. Yoo, & M. C. Wu, Large-scale silicon photonic switches with movable directional couplers. Optica, 2(4), 370-375 (2015).
16. R. K. Gangwar, A. K. Pathak, & S. Kumar, Recent progress in photonic crystal devices and their applications: a review. Photonics, 10, 11, 1199 (2023).
17. N. N. Oza, Y. P. Huang, & P. Kumar, Entanglement-preserving photonic switching: Full cross-bar operation with quantum data streams. IEEE Photonics Technol. Lett.. 26(4), 356-359 (2013).

18. S. Shi, C. Chen, & D. W. Prather, Plane-wave expansion method for calculating band structure of photonic crystal slabs with perfectly matched layers. J. Opt. Soc. Am. A. 21(9), pp.1769-1775 (2004).
19. T. Jalali, K. Rauscher, A. Mohammadi, D. Erni, C. Hafner, W. Baechtold, & M. Z. Shoushtari, Efficient effective permittivity treatment for the 2D-FDTD simulation of photonic crystals. J. Comput. Theor. Nanosci. 4(3), 644-648 (2007).
20. Z. Miao & J. Zhang, Extending Courant-Friedrichs-Lewy stability condition by local eigenvalue perturbation. Geophys. 90(5), 1-58 (2025).
21. Bala, Rajni, and Mrinal Sen. "Optimization of dose parameters for square lattice photonic crystals fabricated via non-dedicated EBL and capacitive coupled RIE for integrated photonic sensors. Mater. Today Commun.. (2026): 114847.